Journal of CO2 Utilization 83 (2024) 102807

Contents lists available at ScienceDirect

Journal of CO2 Utilization

journal homepage: www.elsevier.com/locate/jcou

Towards low-cost and sustainable activated carbon production: Influence of microwave activation time on yield and CO_2 uptake of PET-derived adsorbents

Emmanuel Dan [a], Alan J. McCue [b], Davide Dionisi [a], Claudia Fernández Martín [a,c,*]

[a] School of Engineering, Chemical Processes and Materials Engineering Group, University of Aberdeen, Aberdeen AB24 3UE, United Kingdom
[b] Advanced Centre for Energy and Sustainability (ACES), Department of Chemistry, University of Aberdeen, AB24 3UE, United Kingdom
[c] Centre for Energy Transition, University of Aberdeen, United Kingdom

ARTICLE INFO

Keywords:
Polyethylene terephthalate
Microwave activation
Adsorption
Activated carbon
Carbon capture

ABSTRACT

Microwave (MW) heating is proposed as a method to transform polyethylene terephthalate (PET) into porous adsorbents. The yield, textural properties, and CO_2 uptake of the PET-derived adsorbents irradiated at different durations (3 – 35 min) at 400 °C were assessed. MW activation time influenced both the physical properties and CO_2 uptake capacities of the resulting adsorbents. The yield decreased with activation time, but the surface area, total pore volume, micropore volume, and CO_2 uptake capacities all increased with MW activation time before declining. The optimal sample (produced with 5 min of MW activation time) showed improved textural properties as well as higher equilibrium and dynamic CO_2 uptakes than the commercial activated carbon used as reference. This adsorbent also possesses good selectivity for CO_2 in the binary 10:90%vol/vol CO_2: N_2 mixture. Additionally, an excellent recyclability over 20 cycles, (Regeneration Efficiency > 97%) was observed, and the CO_2 adsorption kinetics best fits Lagergren's pseudo-second-order model. This study has shown that a low activation temperature (400 °C), a short MW activation time (5 min), and a low amount of chemical agent (KOH, 0.72 M) could produce CO_2 adsorbents from a cheap and abundant material (PET-waste) with better CO_2 uptake to that of a commercial activated carbon.

1. Introduction

The continuous buildup of CO_2 concentration in the atmosphere has led to significant changes in the Earth's climate. In 2022, the global concentration of CO_2 emission reached over 36 billion metric tonnes [1], and this value is expected to increase considering the current scenario. The current mitigation strategies, though effective to some extent, are plagued by a wide array of setbacks, most of them the high cost occurred by the increased energy requirement, among other factors. Adsorption using carbon-based adsorbents (CBAs), such as activated carbons (ACs), is effective and materials are inexpensive as they are produced from low-cost and abundant precursors [2].

ACs have been developed from different carbon precursors such as cotton stalk, date stones[3], nut-shell[4], jujun grass and Camellia japonica[5], lotus leaf [6], vine-shoot[7], polyethylene terephthalate [8], bagasse and rice husk [9], melamine-formaldehyde [10], water chestnut shell [11], and urea/petroleum coke [12] for CO_2 capture application. This list has continued to surge, all linked to the inherent advantages associated with preparation and application. ACs possess exceptional textural properties such as a large surface area, high pore volume, thermal stability over a wide range of temperatures, tunable surface chemistry, and the ability to adsorb CO_2 over a wide range of pressures [2]. These characteristics, in addition to their ease of preparation and excellent recyclability over multiple adsorption/desorption cycles, make them more promising materials for CO_2 capture than any other solid adsorbents [13].

Activated carbons are produced by carbonization of carbonaceous precursors at temperatures typically above 400 °C to produce char and subsequent activation of the char to obtain AC using thermal and/or thermochemical treatments. The activation step usually requires a higher energy than the carbonization step, typically 700–800 °C (for chemical activation) [14] and above 800 °C [15] for physical activation

* Corresponding author at: School of Engineering, Chemical Processes and Materials Engineering Group, University of Aberdeen, Aberdeen AB24 3UE, United Kingdom.
E-mail address: cfmartin@abdn.ac.uk (C.F. Martín).

https://doi.org/10.1016/j.jcou.2024.102807
Received 1 March 2024; Received in revised form 23 April 2024; Accepted 17 May 2024
Available online 25 May 2024

to produce ACs of any substantial CO_2 uptake. Aside from the energy input, a typical activation of char to produce AC requires a long duration of more than 4 h [16] for the physical activation and more than 2 h for the chemical activation [17]. The high energy requirement combined with the long activation duration contributes to the increased cost of AC production, in addition to being laborious [18]. A total energy of 14, 000 kJ (4 kWh) is required for the activation of char using a conventional furnace for 2 hours at a power of 2000 W to produce AC [19].

MW-assisted chemical activation (MCA) of char to produce AC is a way to decrease energy requirements [19] and lower the overall cost of producing ACs for carbon capture. Once the char has been obtained from their precursors through carbonisation using a conventional furnace, the MW is then used for the activation using lower energy and a shorter duration. This is because MCA is usually fast and effective at a low bulk temperature due to volumetric heating produced by MW radiation. In MW heating, the thermal gradients are typically less pronounced than those produced by conventional heating [20], with a significant thermal gradient from the inside of the char particle to its cold surface, resulting in energy savings and a shorter processing time [21]. MW temperature distribution during the processing of various materials is demonstrated in different studies [22,23,24]. MCA has been employed in the production of ACs for CO_2 capture from different precursors such as coconut husk [25], tobacco stem [26], pecan nutshell [18], pinewood and wheat straw [19], and oil palm shell [27]. The outcomes of these studies reveal that MCA improved the CO_2 uptake of ACs, reduced production time, and utilised less energy for activation than conventional activation [27]. These demonstrate that MCA produces ACs of comparable or higher CO_2 uptake using a lower temperature (generally around 300–400 °C), shorter activation time (not above 30 mins), and over 10-fold lower energy input than conventional activation [19]

The interaction of MW radiation with materials and the resulting properties varies with several treatment process factors, such as activation time, temperature, and MW power applied. Material response under MW radiation is governed by some factors, such as the dielectric constant (ε'), which refers to the energy storage capacity of a material, and the dielectric loss factor (ε''), which describes the ability of a material to convert MW to heat. The combination of these factors describes the total relative permittivity of a material, also called the MW absorptive capacity [28]. Being that MW heating of materials is complicated and the mechanism is yet to be fully understood [29], the relationship between some treatment process factors used in the activation of char as well as their effects on the properties of the ACs is still not well established. For example, different optimal MW activation times: short (7 min) [30], moderate (15 min) [27], and long (30 min) [19] - have been reported during the preparation of ACs from different precursors. There is still no clear trend of what duration is optimal to produce AC with a specific textural property, yield, or CO_2 uptake due to the difference in the behaviour of MW radiation with materials or the relative permittivity of materials.

Based on the above, there is a research need for sustainable alternative production routes for AC, involving a deep investigation of the parameters of the MW-assisted production treatments that would result in ACs with better properties, such as higher CO_2 uptake and the least energy input given that the process activation conditions impact the adsorption capacity of produced ACs [31]. Optimal production conditions significantly enhance CO_2 absorption in activated carbons (ACs). Coconut shell-based AC, activated at 750°C with a KOH to biochar ratio of 0.5 in a one-step preparation method, achieved the highest CO_2 uptake—5.92 mmol/g at 0°C and 4.15 mmol/g at 25°C [32]. Altering the activator to thiosulphate, with a 700°C activation temperature and a 2:1 thiosulphate to biochar ratio, resulted in uptakes of 5.31 mmol/g at 0°C and 3.59 mmol/g at 25°C [33]. Sulfur-doped ACs, synthesized from polyphenyl sulfide resin using a two-step method, showed optimal CO_2 uptakes of 5.13 mmol/g at 0°C and 3.64 mmol/g at 25°C, with a 650°C activation temperature and a KOH to resin-char ratio of 2 [34]. Similarly, nitrogen-doped ACs from a macadamia nutshell and melamine reached peak uptakes using a 700°C activation temperature and a 2:1 KOH to macadamia/melamine composite ratio [35]. These studies highlight the impact of process parameters on ACs' CO_2 adsorption performance. Incidentally, plastic waste is an attractive alternative to biomass for use as precursors for AC production for CO_2 capture.

Accordingly, using a cheap, abundant, and sustainable waste plastic material, such as polyethylene terephthalate (PET), we have assessed the influence of MW activation time on the yield and CO_2 uptake capacity of an alkaline-impregnated, thermally generated polyethylene terephthalate (PET) char. To the best of our knowledge, there is no report yet regarding the production of ACs from PET waste for CO_2 capture using MW. Neither there are studies focused on the investigation of the influence of MW activation time on the yield and CO_2 uptake capacity of the resultant ACs.

2. Experimental

2.1. Materials

For this investigation, used plastic mineral bottles were collected from local dumpsites around the city of Aberdeen, United Kingdom. A commercial AC (Norit PK1–3) was purchased from Sigma Aldrich in the UK to be used as both a reference material and microwave susceptor. An analytical grade of potassium hydroxide, KOH (ACS reagent, > 85% pellet), was also procured from Sigma Aldrich. Adsorption gases such as carbon dioxide and nitrogen (99.995% purity) were all acquired from BOC Limited, United Kingdom.

2.2. Adsorbent preparation

About 10 g of previously washed pieces of plastic mineral bottles (particle size < 5 mm) were loaded into a quartz jacket (320 mm long with external and internal outlet diameters of 16 and 40 mm, respectively) and placed in a tubular furnace (Nabertherm GmBH RT 50–250/11). The carbonization process was initiated by subjecting the sample to a heating ramp rate of 150 °C/h under N_2 (100 ml/min) up to 600 °C and holding it at 600 °C for 1 h. After carbonization, the sample was allowed to cool down to room temperature under N_2 (100 ml/min). The char was ground using a laboratory mortar to a obtained a powder of particle size less than 1 mm for easy dispersion during chemical activation. The produced char was then chemically activated using KOH. For the activation, 1 g of char was placed in a 0.72 M solution of KOH (prepared by dissolving 1 g of KOH in 25 ml distilled water) and stirred continuously for 8 h at 60°C on a hot plate. The obtained mixture was filtered, and the residue was dried in the oven for 12 h at 105 °C to drive off moisture. For the MW-assisted activation, a mixture of the dried KOH-impregnated char with a 20 g Norit PK (particle size 1–3 mm), a commercial activated carbon used as MW susceptor, was placed in a quartz jacket, and activated at a constant temperature of 400 °C under an N_2 (200 ml/min) in the Flexiwave microwave instrument (MA186–001, from Milestone). The lengths of the MW activation were short (3–5 min), moderate (15 min), and long (25–35 min). Once the activation was completed, the ACs were separated from the MW susceptors using a mesh with an aperture less than 1 mm. There was no observable change in the Norit PK before and after microwave activation. The resulting ACs after MW activation were washed with a 1 M HCl solution followed by distilled water until the wastewater became neutral before they were dried in the oven at 105°C for 12 h. The resultant ACs were named as PET-Y, where 'Y' is the MW activation duration in minutes. The yield was taken as the weight of the AC obtained after MW activation divided by the weight of the char used for activation [25]. As a precautionary measure, the as-purchased Norit PK should be dried overnight prior to activation to drive off moisture to prevent uneven heating profiles or thermal runaway.

2.3. Elemental analysis

The elemental composition analysis for the determination of carbon (C), hydrogen (H), nitrogen (N), sulphur (S), and oxygen (O) contents was carried out using a Thermo Scientific FlashSmart analyser at the University of Birmingham. Before the experiment, the samples were pre-dried in the oven at 90°C for approximately 14 days and stored in airtight sample containers for analysis.

2.4. Adsorbent characterisation and CO_2 adsorption

The adsorbent's textural properties were assessed from nitrogen adsorption isotherms collected using a volumetric sorption analyser (ASAP 2020, Micromeritics) at −196°C after the samples have been degassed at 300 °C for 6 h under N_2 flow. The surface area was determined using the Brunauer-Emmett-Teller (BET) method. For a typical determination of the adsorbent's surface area using the BET method, the N_2 adsorption data was transformed into a linear plot in the partial pressure region $0.05 < P/P^0 < 0.3$, with the slope and intercept of the linear plot used for the determination of the surface area [36]. The total pore volume was calculated at $P/P^0 = 0.49$ from the Horvath-Kawazoe Equation [37], and the micropore volume was calculated using the Dubinin-Radushklevich (D-R) Equation applied to the N_2 adsorption isotherm data.

The narrow micropore volume, average narrow micropore width, and the characteristic energy were calculated using the D-R, Stoeckli-Ballerini, and Dubinin-Astakhov Equations, respectively, from CO_2 adsorption isotherms measured at 0 °C using the same ASAP 2020 sorption analyser. Due to decreased diffusion and kinetic diameter restrictions, nitrogen molecules utilised in adsorption studies at −196°C may not be able to reach the smallest micropores (<0.7 nm) at this temperature. In contrast, CO_2 molecules have a smaller kinetic diameter and greater diffusion rates at higher temperatures (around 0 °C), which allows them to enter these tiny pores more easily. N_2 and CO_2 isotherms were measured after the samples were degassed at 300 °C for 6 hours under N_2. Thermal gravimetry analyses were performed in a thermogravimetric analyser (TGA/DSC 3+, from Mettler Toledo).

The CO_2 adsorption capacities of the prepared adsorbents were assessed under dynamic conditions using a thermogravimetric analyser TGA/DSC 3+ (from Mettler Toledo), while the volumetric sorption analyser (ASAP 2020, from Micromeritics) was used for the determination of the equilibrium adsorption isotherms. The initial dynamic adsorption tests were conducted in 100% CO_2. Future studies are planned under conditions that more closely resemble post-combustion flue gases from natural gas/coal-fired plants, which contain 5/10% vol/vol CO_2, using the optimal sample produced in this study. In a typical dynamic isothermal CO_2 capture experiment, the sample was first dried at 100 °C for 60 minutes under N_2 (50 ml/min) and then maintained at this temperature for 60 minutes to drive off moisture. After drying, the temperature was reduced to 25 °C, and then the feeding gas was changed to CO_2 (50 ml/min) for the adsorption step to commence. The latter was held for 120 minutes to ensure saturation was reached. After the adsorption stage was completed, the regeneration step commenced with a change in the feeding gas to N_2, and with the temperature increasing to 100°C. Afterward, the sample was cooled to 25°C under N_2, preparing the sample for the next adsorption-regeneration cycle to begin. This was repeated 20 times for the adsorbent's cyclability test. The quantity of CO_2 adsorbed or desorbed by the sample was calculated from the mass-time data obtained from either the adsorption or desorption steps using the gravimetric method described in detail elsewhere [38]. The total amount of CO_2 adsorbed and desorbed by the adsorbents was evaluated using Eqs. 1 and 2, respectively. The stable working capacity defined as the adsorbent's effective capacity of adsorption/desorption in the adsorption and desorption cycles [39] was also elucidated from the adsorption/desorption data.

$$Total\ amount\ of\ CO_2\ adsorbed\left(\frac{mmol}{g}\right) = \sum_{n=1}^{n=20}(C_1 + C_2 + \ldots.. + C_n) \quad (1)$$

where C_1 and C_2 …. Cn represents the amounts of CO_2 adsorbed in cycles 1, 2, …n in mmol/g.

$$Total\ amount\ of\ CO_2\ desorbed\left(\frac{mmol}{g}\right) = \sum_{n=1}^{n=20}(D_1 + D_2 + \ldots.. + D_n) \quad (2)$$

where D_1 and D_2 …. D_n represents the amounts of CO_2 desorbed in cycles 1, 2, …n in mmol/g.

On the other hand, the maximum CO_2 uptake of the adsorbents under equilibrium conditions was elucidated from the CO_2 isotherm measured at different temperatures (0, 25, 50 °C), and up to 1 bar. The isosteric heat of adsorption (Q_{st}) of CO_2 for the adsorbent was calculated from the CO_2 isotherms at different temperatures using the Clausius-Clapeyron equation [40]. To assess the CO_2 selectivity of the prepared adsorbent over N_2, the Ideal Adsorption Solution Theory (IAST) was applied to the sample N_2 isotherms at different temperatures based on Henry's law (see Eq. 3) [41].

$$S_{i,j} = (q_i/p_i)\Big/(q_j\Big/p_j) \quad (3)$$

where q_i, *and* $q_j$and $p_i and p_j$ represent the adsorption uptakes and partial pressures of components i and j.

2.5. Modelling of CO_2 adsorption isotherm

Langmuir, Freundlich, and Sip adsorption models were used to fit the experimental adsorption isotherm results obtained for the adsorbent using the Excel solver function. These adsorption isotherm models are well-known, with their theories and assumptions already explained in detail elsewhere [42]. The mathematical equations for Freundlich, Langmuir, and Sip used in this study, with an explanation of each parameter, are presented in Eqs. 4–6, respectively.

$$Q_0 = K_F(C_e)^{\frac{1}{n}} \quad (4)$$

Q_0 represents the CO_2 concentration (mmol/g), C_e is the CO_2 pressure concentration (kPa), K_F is the Freundlich constant (mmol/(g·kPa$^{-1/m}$) and 1/n is the heterogeneity factor which is a dimensionless constant.

$$Q_e = \frac{Q_o K_L C_e}{1 + K_L C_e} \quad (5)$$

Q_0 represents the theoretical monolayer capacity (mmol/g), K_L is the Langmuir isotherm constant (kPa/mmol) and depends on the adsorbent-adsorbate interaction, Q_e is the amount of an CO_2 on the surface in equilibrium.

$$q = \frac{q_{mS} b p^n}{1 + \quad bp^n} \quad (6)$$

where q_{mS} is a constant reflecting maximum adsorption capacity (mmol/g), b is the Sips constant (bar^{-1}), and n is the heterogeneity factor (a dimensionless constant).

The goodness of fit of these kinetic models with the experimental data was assessed based on the nonlinear coefficient of determination (R^2), which was evaluated using Eq. 7. The difference between the experimental data and predicted values from the models (i.e., the residual sum of squares) denoted as Δq was computed using Eq. 8.

$$R^2 = 1 - \left(\frac{\sum_{i=1}^{n}\left(q_{t,\exp} - q_{(t,model)}\right)^2}{\sum_{i=1}^{n}\left(q_{t,\exp} - q_{t,exp^-}\right)^2}\right) \times \left(\frac{n-1}{n-p}\right) \quad (7)$$

where $q_{t,\ exp}$ is the experimental value, $q_{t,\ model}$ is the predicted value

from kinetic models, q_{t,exp^-} is the average value of the experimental data, n is the number of experimental data points fitted in the model, and p represents the number of parameters of the model.

$$\Delta q(\%) = \sqrt{\frac{\sum_{i=1}^{n}\left(q_{t,\exp} - q_{t,model}\right)_i^2}{n-1}} \times 100 \quad (8)$$

where $q_{t,\ exp}$ is the experimental value, $q_{t,\ model}$ is the predicted value from adsorption isotherm model, and n is the number of experimental data point fits in the adsorption model.

2.6. CO_2 adsorption kinetics

Three empirical kinetic models, namely Lagergren's pseudo-first order, pseudo-second order, and Avrami's model, were used to assess the kinetics of CO_2 adsorption by the prepared adsorbent. These models have been widely used to predict the adsorption kinetics of CO_2 on different carbon-based materials, including activated carbons [43,44]. In Lagergren's pseudo-first order, the adsorption system is viewed as a system where the adsorption rate is proportional to the number of available active sites [45]. The model is useful in predicting the physical adsorption of CO_2 on solid adsorbents, and it signifies a reversible interaction between the adsorbent and adsorbate. The integrated form of the model used in this study is shown in Eq. (9) [46].

$$q_t = q_e\left(1 - e^{-k_1 t}\right) \quad (9)$$

where q_t is the CO_2 adsorbed (mmol/g) at time t (min), q_e is the CO_2 adsorbed at equilibrium (mmol/g) and k_1 (min^{-1}) is the first order rate constant.

Lagergren's pseudo-second order assumes there is a strong bond between the adsorbate and the adsorbent. Unlike the pseudo-first-order model, this model represents a system whose adsorption rate is proportional to the square of the adsorption sites present on the surface of the adsorbents. The equation for the model is presented in Eq. 10.

$$q_t = \frac{q_e^2 K_2 t}{1 + q_e K_2 t} \quad (10)$$

where q_t is the CO_2 adsorbed (mmol/g) at time t (min), q_e is the CO_2 adsorbed at equilibrium and k_2 (mmol/g/min) is the second order rate constant.

Avrami's fractional-order kinetic model was also used to assess the behaviour of CO_2 adsorption by the prepared adsorbent. Although this model was originally developed to mimic crystal formation and a material's change of state, it has found usefulness in the study of gas adsorption on solids [45]. The mathematical form of Avrami's model is represented in Eq. 11.

$$q_t = q_e\left(1 - e^{-kt^n}\right) \quad (11)$$

where q_t is the CO_2 adsorbed (mmol/g) at time t (min), k (g/(mmol min)) is the Avrami's kinetic constant, and n is the Avrami's exponent. The goodness of fit of the models with experimentally obtained data was also assessed based on the nonlinear coefficient of determination (R^2), as shown in Eq. 7.

3. Results and discussion

After the MW activation of PET char with the aid of Norit PK1–3 as the MW absorber, the physical appearance of the resulting material (microwave PET-ACs) was a shiny granulated substance of particle size < 1 mm.

3.1. Yield, textural properties, and dynamic CO_2 uptake of microwave activated PET-ACs

The yield of the prepared ACs ranged from 81% to 96% (Table 1), with the highest yield (96%) obtained for sample PET-3, while the lowest (81%) was obtained for sample PET-35. The result shows that as activation time increases, the yield of AC decreases. Fig. 1a represents the plot of mass loss (wt%) against temperature for all the ACs, with the derivative TG plots depicted in Fig. 1b. The thermal decomposition profiles of the ACs are similar having two pronounced peaks of weight loss with similar rates, but different intensities in the temperature ranges: 25–180 °C and 625–1000 °C. A third peak of weight loss is observed in the range 180–420 °C with greater intensity for sample PET-35. Weight loss occurring in the temperature range 25–180 °C is attributed to the loss of pre-adsorbed water and/or CO_2 molecules, while the loss in the range 200–400°C is likely that of surface carboxylic acids (strong and weak types) [47], and the loss observed in the range of 625–1000 °C is attributed to the loss of oxygenated groups such as hydroxyl (-OH) and carbonyls [47] that were formed during the impregnation of PET char with KOH and subsequent activation. The total weight loss for each AC over the temperature range of 25–1000 °C is displayed in Table 1. A trend of decreasing weight loss with increasing activation time was observed, though it was discontinued when activation time was increased from 25 to 35 minutes. The highest weight loss (6.19%) was obtained for sample PET-35, while the lowest (5.07%) was obtained for sample PET-25. However, the ACs were stable over the tested temperature range (25–1000°C), with total weight losses lower than 7%.

The N_2 isotherms at −196°C for the MW-activated PET-ACs are shown in Fig. 1(c). All the prepared samples exhibit a type I isotherm suggestive of microporous adsorbents [48]. A plateau was observed with no significant increase in the volume of N_2 adsorbed by the samples at higher relative pressures than 0.1, indicating that the adsorbents were entirely composed of micropores. The BET surface area, total pore volume and micropore volume first increased when the activation time was changed from 3 to 5 minutes before declining when the activation time was further prolonged from 5 to 35 minutes (see Table 1). The results show that the optimum textural properties were achieved at an activation time of 5 minutes.

The maximum CO_2 uptake of the ACs under dynamic conditions is shown in Table 1, while the variation of the AC's CO_2 uptake with the activation time is given in Fig. 1d. The CO_2 uptake increased from 1.67 to 1.80 mmol/g when the activation time was increased from 3 to 5 min, before reducing with further increases in activation times. This is because, under prolonged microwave heating, micropores are enlarged, thus increasing the average narrow micropore width (L_0) (see Table 1), and the local hot spots produced on further MW heating led to the destruction of the carbon surface, thereby limiting the CO_2 molecules from gaining access to the functional sites and resulting in reduced CO_2 adsorption [25]. PET-5 is the sample with the lowest average narrow micropore width (0.54 nm) and the greatest CO_2 uptake under dynamic conditions (1.80 mmol/g). For reference, the dynamic CO_2 uptake by the optimal sample prepared in this study is higher than that reported for (i) mixed plastic-derived AC (1.53 mmol/g) [49], (ii) microcrystalline cellulose-derived adsorbent (1.59 mmol/g) [50] and (iii) commercial AC Norit PK1–3 (1.65 mmol/g) (dynamic capture capacity was measured in this study under the same conditions).

A shorter MW activation duration helps in gaining extra active sites by opening previously closed pores and creating new ones through selective activation [25]. As the activation duration exceeds the optimum, the AC's surface area reduces because a further increase in activation time results in uneven activation, leading to the destruction of some pores and thereby decreasing the surface area [25,26], From the CO_2 isotherms at 0 °C (see Table 1 and Fig. 2a), the volume of narrow micropores (pores < 1 nm) was found to follow the same trend conveyed from the N_2 isotherm data, with the PET-5 sample having the highest

Table 1
Yield, textural properties, and dynamic CO_2 uptake performance of MW-activated PET-ACs.

Sample	Yield (%)	Total wt. loss (%)	N_2 Isotherm			CO_2 Isotherm			Dyn. CO_2 uptake (mmol/g)[g]
			S_{BET}[a] (m^2/g)	V_t[b] (cm^3/g)	$W_{0,\ N2}$[c] (cm^3/g)	$W_{0,\ CO2}$[d] (cm^3/g)	L_0[e] (nm)	E_0[f] (KJ/mol)	
PET char	-	5.06	-	-	-	-	-	-	0.91
PET-3	96	6.18	373	0.14	0.14	0.23	0.62	28.92	1.67
PET-5	93	6.05	450	0.18	0.18	0.24	0.54	31.27	1.80
PET-15	91	5.26	353	0.14	0.14	0.23	0.63	28.17	1.54
PET-25	85	5.07	252	0.10	0.10	0.19	0.61	29.19	1.51
PET-35	81	6.19	228	0.09	0.09	0.19	0.68	27.20	1.35

[a] BET surface area.
[b] total pore volume.
[c] total micropore volume.
[d] narrow micropore volume (pore width < 1 mm).
[e] average narrow micropore width.
[f] characteristic energy.
[g] maximum dynamic CO_2 uptake at 25°C.

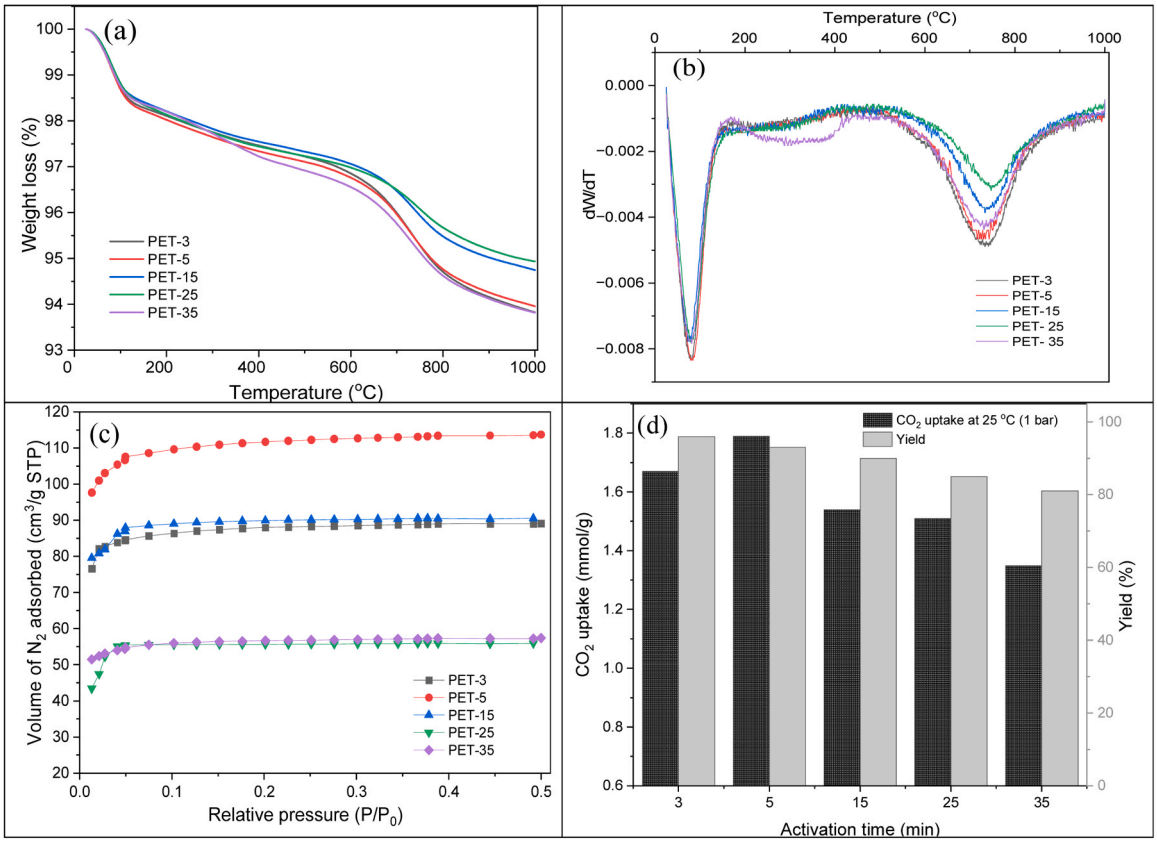

Fig. 1. TG (a) and DTG (b) plots; N_2 adsorption isotherm at −196°C of MW-activated PET-ACs (c); correlation between CO_2 uptake and yield with MW activation time (d).

narrow micropore volume (0.24 cm^3/g). The average narrow micropore width (L_0) ranged between 0.54 and 0.68 nm for all the prepared ACs. The result reveals that the least narrow pores (0.54 nm) were obtained in sample PET-5, which was reflected in increased characteristic energy (E_0).

3.2. CO_2 adsorption isotherms

The CO_2 isotherm data collected at temperatures between 0 and 50°C are depicted in Fig. 2. The maximum adsorption capacities under equilibrium are summarised in Table 2. The maximum equilibrium uptake displayed a similar trend to the one found with the dynamic CO_2 uptake for all the temperatures (Table 1). Sample PET-5 exhibited the highest CO_2 uptake, while the lowest uptake was recorded for sample PET-35. This may be attributed to the improved textural properties shown by PET-5 (Table 1). Interestingly, the maximum equilibrium uptake displayed by all the produced microwave-activated PET-ACs is comparable to or higher than some previously reported CO_2 adsorbents [38,51,52], This is of particular importance as the ACs from this work are prepared using a low concentration (0.72 M) of the chemical agent KOH. The CO_2 uptake capacities decreased with increasing temperature for all the ACs, confirming that CO_2 adsorption onto the ACs is exothermic and likely via physisorption [12]. The plot of maximum equilibrium uptake with temperature for all the ACs is represented in

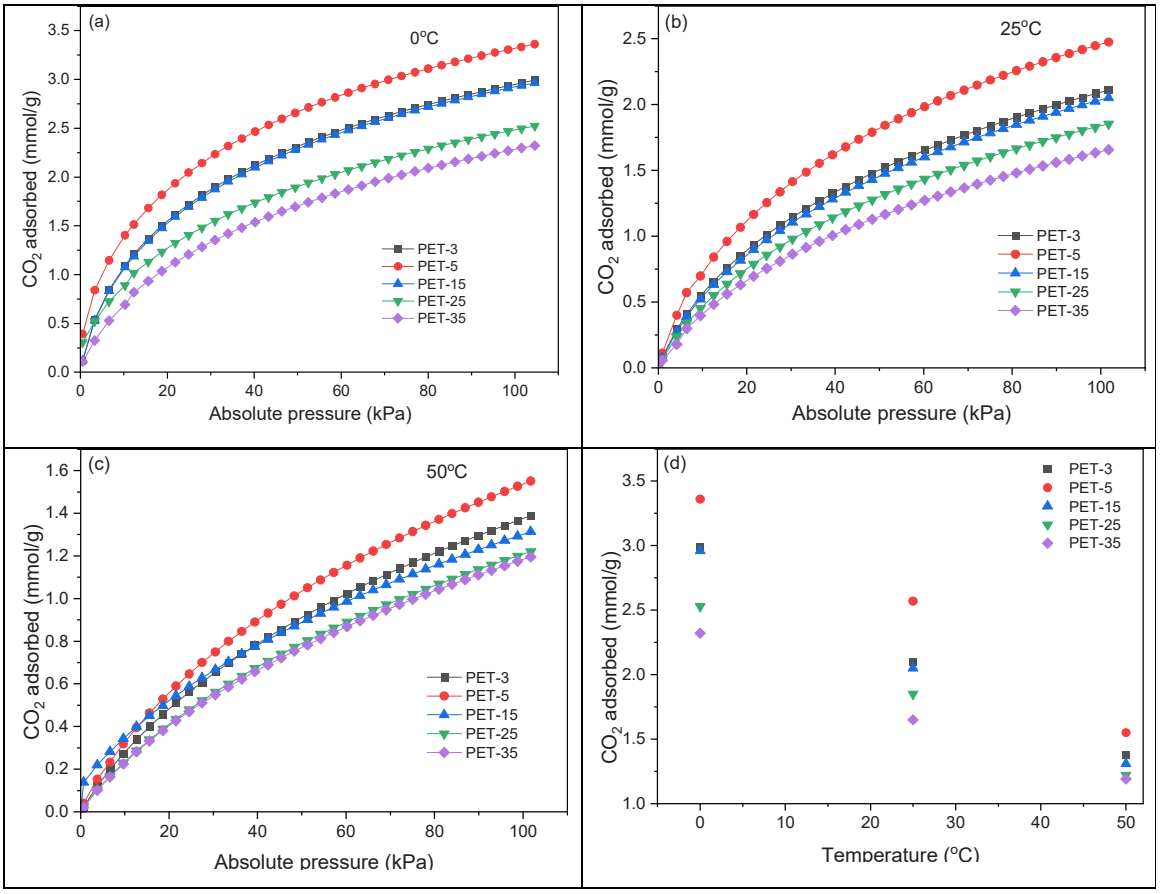

Fig. 2. CO_2 adsorption isotherms of MW-activated PET-derived ACs, measured at (a) 0 °C, (b) 25 °C, and (c) 50 °C; (d) CO_2 uptake at different temperatures and 100 kPa.

Table 2
Maximum equilibrium uptake of MW-activated PET-ACs at different temperatures.

Sample	CO_2 isotherm (mmol/g)[a]		
	0 °C	25 °C	50 °C
PET-3	2.99	2.10	1.38
PET-5	3.36	2.57	1.55
PET-15	2.96	2.05	1.31
PET-25	2.53	1.85	1.22
PET-35	2.32	1.65	1.19

[a] obtained at 1 bar using volumetric sorption analyser.

Fig. 2d. The observed decrease in CO_2 uptake by these ACs with increasing temperature may be explained by the fact that as temperature increases, the kinetic molecular energy of the adsorbate (CO_2) becomes greater, thereby allowing for the escape of the molecule from the surface of the ACs [18,46].

Next, the relationship between the textural properties and the CO_2 uptake capacities of the prepared ACs at 25°C and 100 kPa was assessed. The plots of CO_2 uptake against some textural parameters taken from Table 1, such as the BET surface area (S_{BET}), total pore volume (V_t), micropore volume ($W_{0,\ N2}$), narrow micropore volume ($W_{0,\ CO2}$) and the average narrow micropore width (L_0) are presented in Fig. 3. These results show that there is a good correlation between the CO_2 uptake by the prepared adsorbents and each of the textural properties plotted against. The CO_2 uptake shows a positive correlation with the increase of AC's surface area, total pore volume, micropore volume, and narrow micropore volumes (Fig. 3a-d). For the average narrow micropore width (L_0), however, it was observed an increase in the CO_2 uptake with the decrease in the L_0 values (Fig. 3e). This agrees with the reported by Martín et al [53], and that for the same L_0 value, other parameters such as the ones mentioned earlier have the greatest impact on the CO_2 uptake.

According to these correlations, the CO_2 uptake of the PET-ACs is shown to be determined by a combination of the BET surface area, V_t, $W_{0,\ N2}$, $W_{0,\ CO2}$, and L_0, and especially by the $W_{0,\ N2}$ (as samples' pores were mainly microporous) and L_0. This was evidenced by the fact that samples PET-3 and PET-15, despite having the same total pore volume (V_t), micropore volume ($W_{0,\ N2}$), and narrow micropore volumes ($W_{0,\ CO2}$), only differing by the size of the average narrow micropore width (L_0), were found to display different CO_2 uptakes. A low CO_2 uptake capacity was displayed by samples with L_0 in the range of 0.6–0.63 nm and lower $W_{0,\ N2}$, and V_t. However, the samples irradiated for 5 minutes showed the highest S_{BET}, V_t, $W_{0,\ N2}$, and $W_{0,\ CO2}$, but the lowest L_0 was found to have the highest CO_2 uptake. The importance of textural properties such as the volume of narrow micropores (diameter < 1 nm) [4], micropore volume [8], surface area and pore volume [5], the average narrow micropore width [7], and combinations of two or more textural properties [6] to govern the CO_2 uptake of adsorbents at low temperatures (25 °C) and pressure (1 bar) have been reported in the literature. Under the mentioned conditions, the parameters which govern the CO_2 uptake the most are narrow micropore volume ($W_{0,\ CO2}$) and the average micropore width (L_0) [54].

From the results presented, samples that were irradiated with MW for a short time of 5 minutes exhibited improved textural properties and produced the optimal CO_2 uptake capacity in both dynamic and equilibrium conditions, compared to those activated for a longer time. Therefore, 5 minutes of MW activation time was required to produce AC with optimal CO_2 uptake from PET, using a less concentrated KOH

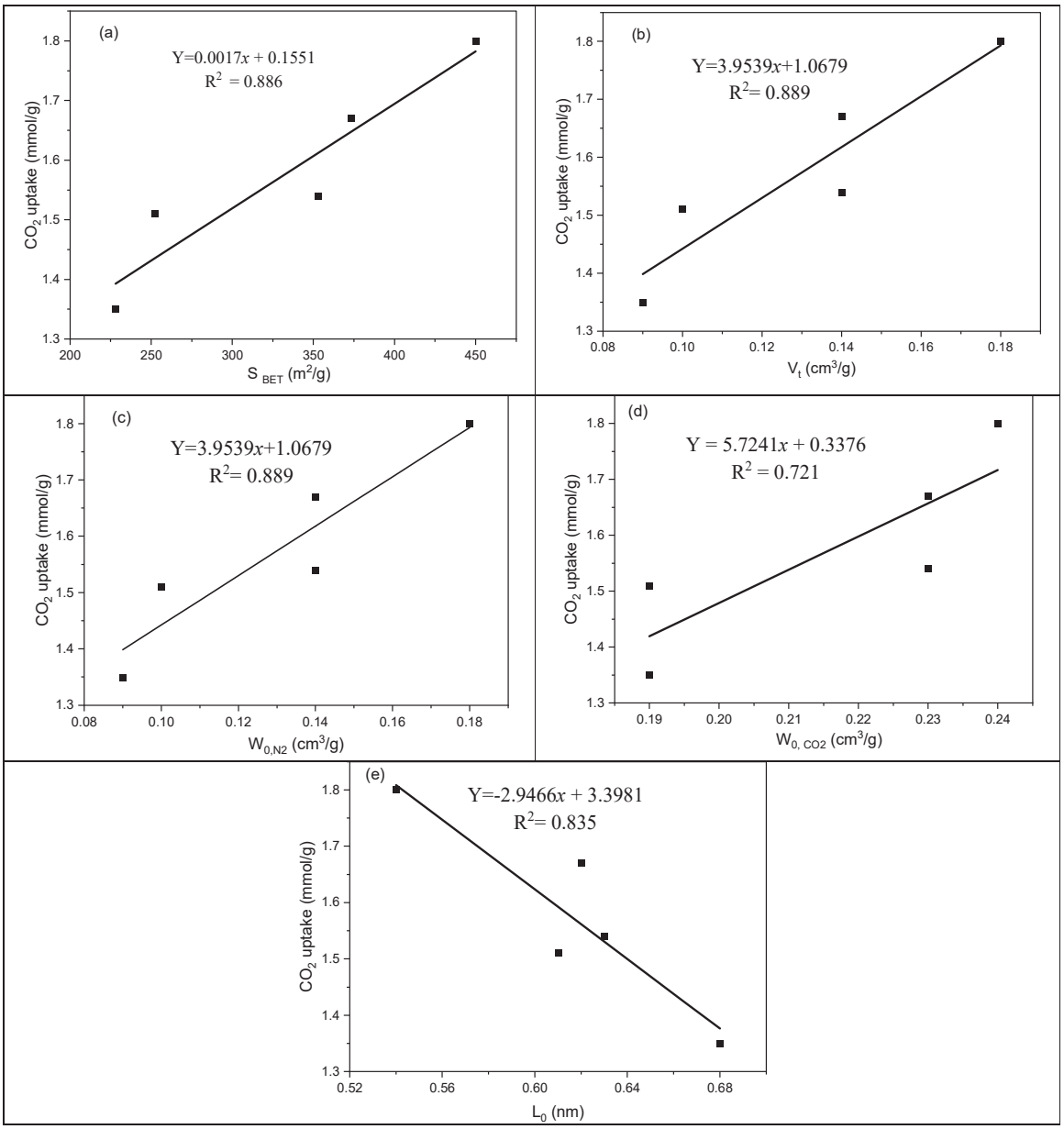

Fig. 3. Correlation between CO_2 uptake against (a) BET surface area (b) total pore volume (c) micropore volume (d) narrow micropore volume, and (e) narrow micropore width.

solution (0.72 M) compared to 2.84 M for chicken-manure derived AC [55], and 3.55 M for empty fruit brunch-derived AC [56]. The use of less activating agent (KOH) is of great benefit, as this would contribute to reducing the cost of AC production, cut down on washing time and potentially reduce water consumption following chemical activation. As a result, the PET-5 sample was chosen as the reference sample for further analysis.

3.3. Elemental analysis

The elemental composition of PET char obtained from the thermal carbonisation of PET plastics and the MW-activated PET char (PET-5) are displayed in Table 3. From the results, the carbon and hydrogen contents of the PET char were higher than those obtained for the MW-activated sample. The observable decrease in carbon and hydrogen contents may be due to the release of volatile compounds during the activation of PET char [57]. The results show that PET char and MW-activated char contained no sulphur, however, the MW-activated sample was found to contain some amount (0.37 wt%) of nitrogen when compared to the composition of its parent char (no nitrogen content). The presence of nitrogen in MW-activated PET char could arise from the complex interaction of MW with species such as KOH and the surface functionalities present in the activated carbon, all in the presence of N_2 gas. This observation agrees with the reported by Biti et al

Table 3
Elemental composition (wt%) of PET-char and the 5-min MW-activated PET char.

Sample	C	H	N	S	O[a]
PET-char	91.05	3.28	0.00	0.00	5.67
PET-5	82.73	1.26	0.37	0.00	15.64

[a] obtained by difference.

[58], as they also identified the presence of Nitrogen in the MW-activated microcrystalline cellulose-derived ACs despite Nitrogen not being present in the parent biochar. This was attributed to the micro plasma hot spots developed from MW heating under a nitrogen environment. This reaction is believed to occur through a free radical mechanism and has been explained in detail elsewhere [59]. The higher oxygen content in the MW-activated sample than in the PET char is attributed to the KOH activation process. During the chemical activation of the char, metal oxides decompose into oxides within the carbon matrix, thereby aiding oxidation and the creation of more oxygenated moieties [60,61].

3.4. Isosteric heat of adsorption and CO_2/N_2 IAST selectivity

The isosteric heat of adsorption (Q_{st}) of CO_2 on sample PET-5 was found to range from 32.9 to 39.1 kJ/mol over a CO_2 loading range of 0.15–1.20 mmol/g. The values for the Q_{st} for all temperatures (0, 25, and 50 °C) were higher at the beginning of adsorption (lower CO_2 loading) and became smaller as loading increased (Fig. 4a), showing a possible multilayer adsorption and the strengthening of intermolecular interactions between CO_2 and the ACs. This observation, which has been reported previously, indicates that the ACs produced possess a heterogeneous energy surface with multiple adsorption sites [12]. The Q_{st} values reported in this study are comparable to or higher than those reported for polyvinylidene fluoride and rice-husk derived ACs (21.3–24.2 kJ/mol) [62] and 20.8–18.55 kJ/mol [63], respectively. The relatively high Q_{st} displayed by sample PET-5, an average of 34.59 kJ/mol for the tested temperatures, compares to the typical average value for the same type of samples, i.e., highly microporous ACs [64] which may be related to the low average micropore width and high volume of narrow micropores that PET-5 was shown to possess (see Table 1), which results in stronger interactions between the CO_2 molecules and the adsorbent's surface [18].

For an adsorbent to be considered for carbon capture application, it is highly desirable to exhibit a selective uptake of CO_2 over other gases. The selectivity of CO_2 over N_2 for sample PET-5 was calculated from the pure CO_2 (see Fig. 2c) and N_2 isotherms (Fig. 4b) measured at different temperatures (0, 25, and 50 °C), using the IAST selectivity model (Eq. 3). For all temperatures, the volume of CO_2 adsorbed by the sample was higher than that of N_2, as shown by their pure isotherms. The selectivity of CO_2 over N_2 was assessed for a typical flue gas mixture consisting of CO_2 and N_2, 10:90% vol/vol[65]. Under these conditions the selectivity of CO_2 over N_2 obtained for PET-5 were 29.3, 35.1, and 39.7 for 0, 25, and 50 °C, respectively. The increase in selectivity observed with increasing adsorption temperature (Fig. 4c) could be due to the larger difference between the amount of CO_2 and N_2 adsorbed by the sample at different temperatures. Increasing CO_2 selectivity over N_2 with increasing adsorption temperatures has also been attributed to the presence of oxygen containing functional groups like hydroxyls and carbonyls on the AC's surface [66] as evidenced by the oxygen contents revealed by the elemental analysis (see Table 3). The trend obtained for selectivity with temperature is consistent with the literature [10,66] and the values obtained are consistent with those reported for other CO_2 adsorbents for the same gas composition [11,63,65].

3.5. CO_2 adsorption-desorption cycle under dynamic conditions

Although PET-5 exhibited excellent dynamic isothermal CO_2 capture capability, which is a significant factor in the selection of good adsorbents [62], the ability for adsorbents to be easily regenerated with high cyclic stability over repetitive cycles (each cycle comprises adsorption and desorption steps) is also crucial. This is of great importance as it

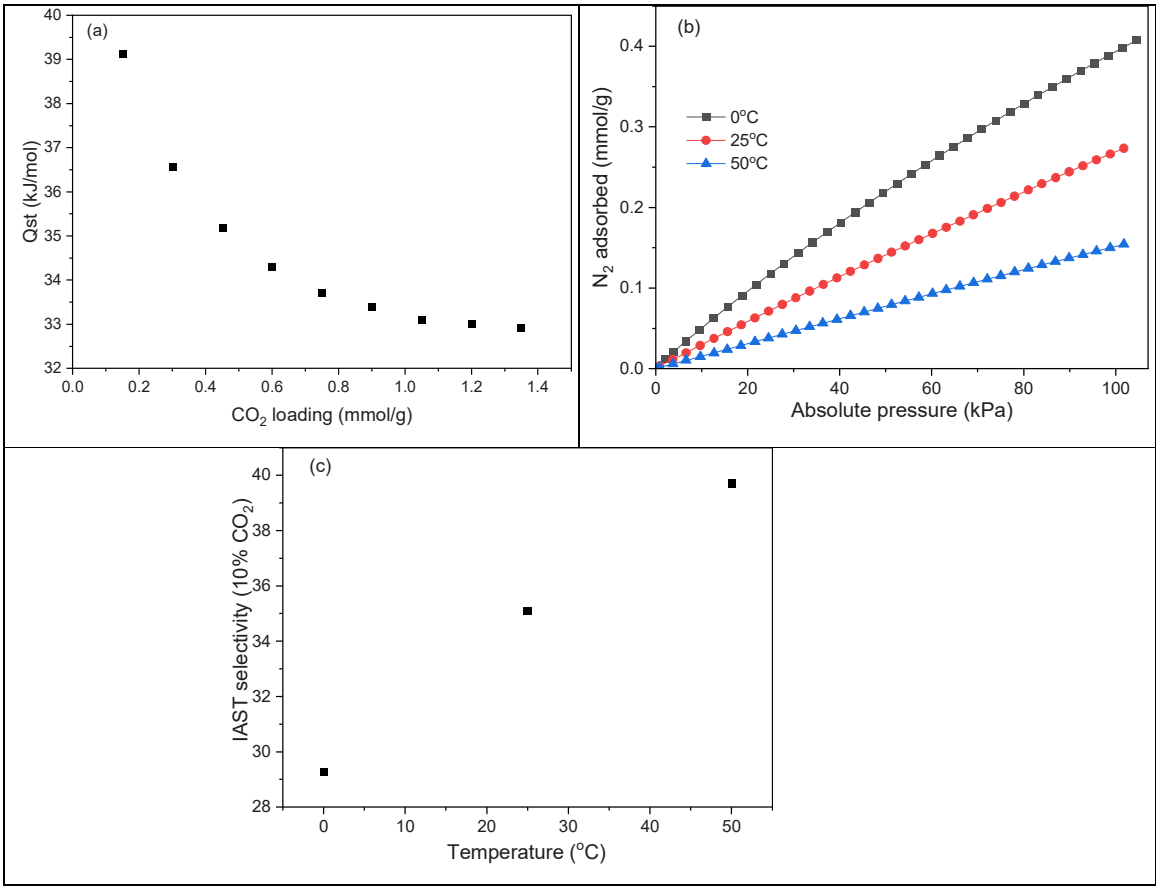

Fig. 4. (a) Q_{st} against CO_2 loading, (b) N_2 isotherms at different temperatures, and (c) IAST selectivity of PET-5 sample.

would provide useful insight into potential stability under dynamic process conditions, desorption behaviour of the ACs, energy requirement for regeneration and by extension the associated operational cost in a typical carbon capture process. The CO_2 cyclic performance for PET-5 was measured over 20 cycles in the TGA as described in the experimental section. Fig. 5a depicts the 20 CO_2 adsorption-desorption cycles, while Fig. 5b displays the maximum dynamic CO_2 uptake for each cycle against the cycle number. The total amount of CO_2 adsorbed over the 20 cycles was 30.94 ± 0.01 mmol/g, with a stable working capacity of 1.55 mmol/g, whereas a total of 28.65 ± 0.00 mmol/g CO_2 was desorbed, with 1.43 mmol/g CO_2 desorbed during each single desorption cycle.

Using the adsorption and desorption data from the TGA, we quantified the adsorbent's desorption and regeneration efficiencies. Desorption Efficiency (DE) was calculated using Eq. 11, while the Regeneration Efficiency (RE) was calculated using Eq. (12)[67].

$$DE = q_{des}/q_{ads} \times 100 \quad (12)$$

where q_{des} is the amount of CO_2 desorbed per cycle, and q_{ads} is the amount adsorbed in each cycle.

$$RE = q_i/q_o \times 100 \quad (13)$$

where q_i is the amount of CO_2 adsorbed in other cycles, and q_o is the amount adsorbed in the first cycle.

The CO_2 desorption and regeneration efficiencies of sample PET-5 against cycle number are displayed in Fig. 5c. The sample's desorption efficiency over the whole 20 cycles ranged from 90.36% to 92.93%, with individual cycles recording DE of above 92% except the first (90.36%). The difference between the DE of the first cycle and the rest of the cycles is due to the higher CO_2 adsorbed and desorbed in the first cycle, when the sample was fresh, compared to those of the other cycles. The regeneration efficiency (RE) ranged from 99.24% to 100% (with the exclusion of cycle 1). With the inclusion of cycle 1, RE ranged from 97.84% to 100%, with an average RE of 97.99 ± 0.19%, and each cycle exhibiting RE not below 97%. If cycle 1 is ignored, RE ranges from 99.24% to 100%, and an average of 99.37 ± 0.12% RE is reported. The slight changes in RE (< 1% when cycle 1 is excluded) within the entire 20 cycles may be due to the experimental procedures, which may not have been optimal [67].

3.6. CO_2 adsorption kinetics

To assess the CO_2 adsorption dynamics of the prepared adsorbent and its suitability for a real-world application, the dynamic isothermal CO_2 uptake data was fitted with three kinetic models as described previously.

Fig. 6 shows the predicted CO_2 capacities from the three kinetic models for sample PET-5 at 25 °C fitted with experimental data obtained from the TGA. The values for the kinetic parameters from the models investigated, the error values from different error models adopted, as well as the nonlinear correlation coefficients are summarised in Table 4. For the uptake, it was observed that most of the adsorption took place within the initial 20 minutes, during which 95% of the total CO_2 maximum uptake at equilibrium (i.e., the end of the adsorption) was achieved as indicated in Fig. 6.

The experimental data fitted better with the pseudo-second-order model at all stages of adsorption compared to the fit obtained for both the pseudo-first-order and Avrami models (see Fig. 6). The pseudo-second order model showed the lowest sum of the square error (SSE)

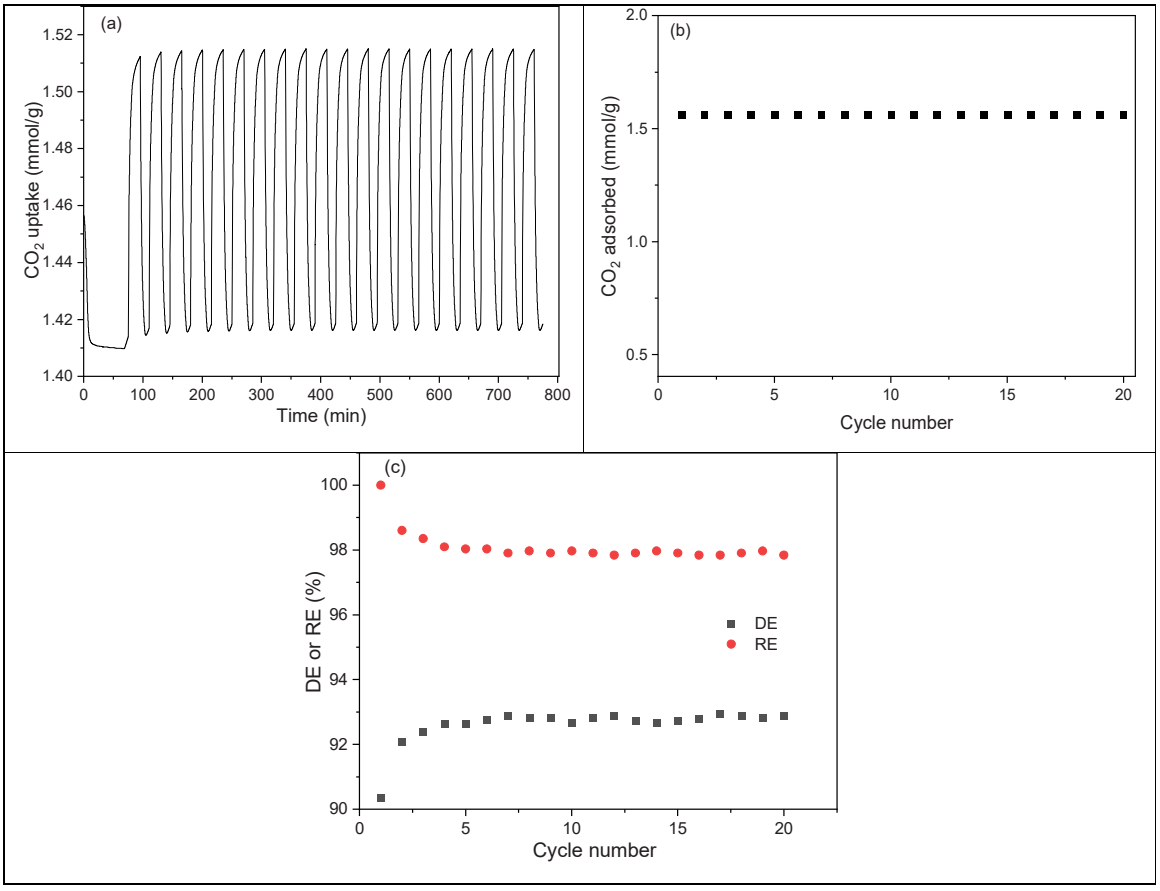

Fig. 5. (a) CO_2 cyclic stability test at the constant adsorption temperature of 25 °C with N_2 purge for desorption at 100 °C; (b) maximum dynamic CO_2 adsorption for each cycle against cycle number; and (c) CO_2 desorption and regeneration efficiencies for PET-5.

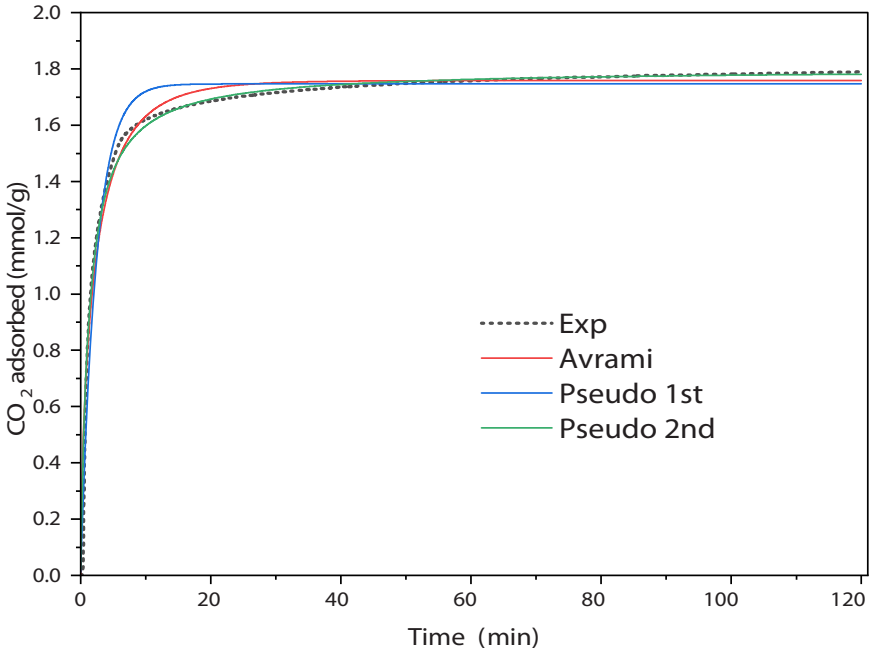

Fig. 6. Kinetics of CO_2 uptake on PET-5: Experimental and predicted dynamic capacities at 25 °C.

and average relative error (ARE) values, the greatest R^2, and predicted a CO_2 uptake at equilibrium which was identical to the experimental value (1.80 mmol/g) (see Table 1). To further ascertain if the pseudo-second-order model was applicable in the adsorption of CO_2 on the prepared AC, a plot of t/qt against time resulted in a straight-line graph from the origin with a coefficient of linear regression (R^2) of 1 (see supplementary information), confirming the adsorption process followed a pseudo-second order model[68]. This implies that CO_2 adsorption on PET-5 is governed by a physisorption process. Both Avrami and the pseudo-first-order models displayed similar trends, with both models fitting well with the experimental data at the initial phase of adsorption but overestimating and underestimating at the later and equilibrium stages, respectively. The rate constants, K, for the kinetic models, were 0.42 min^{-1} for the pseudo-first-order, 0.44 g/mmol/min for the pseudo-second-order, and 0.58 min^{-1} for Avrami's model. The values of K for the pseudo-first and pseudo-second-order models were similar. For the best fitting kinetic model (i.e., pseudo-second-order), the value of K (0.44 min^{-1}) obtained for the adsorbent in this study is 11-fold higher than 0.04 min^{-1} for palm solid waste-derived AC [69] and 12-fold higher than 0.036 min^{-1} for pinecone-derived AC [70] reported for the adsorption of CO_2. This indicates that, compared to palm solid waste or pinecone-derived ACs, the adsorption of CO_2 by MW-activated PET-derived AC is faster, which is quite outstanding as a smaller quantity of this adsorbent would be required to capture a given volume per unit time [39]. To be emphasized, the adsorption of CO_2 on the prepared AC was observed to be significantly faster—11 times more than phenols on bagasse fly ash [71], and 31 times more than methane on palm kernel shell-derived ACs [72]—even though those ACs were specifically developed for adsorbing those molecules. This indicates a notably slower adsorption rate for phenols and methane despite their targeted design.

Table 4
Kinetic model parameters of CO_2 adsorption on sample PET-5.

Model	Kinetic parameters	Temperature	Error models		
		25 °C	SSE	ARE	R^2
Avrami	n	0.65	8.93	58.24	0.96
	K_A (min^{-1})	0.58			
	$q_{e\ exp}$ (mmol/g)	1.80			
	$q_{e\ cal}$ (mmol/g)	1.76			
Pseudo-1st order	K_f (min^{-1})	0.42	14.78	21.92	0.93
	$q_{e,\ exp}$ (mmol/g)	1.80			
	$q_{e,\ cal}$ (mmol/g)	1.75			
Pseudo-2nd order	K_s (g/(mmol min))	0.44	3.85	18.36	0.98
	$q_{e\ exp}$ (mmol/g)	1.80			
	$q_{e\ cal}$ (mmol/g)	1.80			

$q_{e\ expt}$ obtained from TGA result, $q_{e\ cal}$ kinetic model using Excel solver, SSE – sum of squares of the error, ARE- average relative error, R^2 – nonlinear correlation coefficient.

3.7. CO_2 adsorption isotherms modelling

Whilst it is important to assess the behaviour of the prepared AC under dynamic conditions as presented earlier, it would also be beneficial to evaluate the adsorption capacity of the AC under equilibrium conditions determined in terms of the volume of gas adsorbed and assessed using adsorption isotherm models. This would provide some information, such as the AC's surface features and the adsorption capacity at equilibrium. As stated previously, three adsorption isotherm models, namely Freundlich, Langmuir, and Sips, were adopted for the characterisation of the CO_2 adsorption isotherms measured.

Fig. 7 displays the CO_2 adsorption isotherms at different temperatures (0, 25, 50 °C) fitted to different isotherm models for PET-5. Table 5 summarises the model parameters' values, the goodness of fit (based on the nonlinear correlation coefficient (R^2), and the residual sum of squares between the model's predicted CO_2 uptake and the experimental uptake Δq (%)) obtained from the fit of each model to the experimental data based on Eq. 8.

Sips model fitted the experimental data well, with the value for the R^2 close to unity and the lower percentage of the sum of the residual square error calculated for all temperatures. The values obtained for the Sips parameter (n) for all the temperatures were greater than 1. The Sips parameter usually defines the heterogeneity or homogeneity of an adsorbent's surface, with a value greater than unity indicating heterogeneity [73]. Based on this, it can be confirmed that the AC's surface is heterogeneous. This agrees with the trend observed previously on the varying values of Q_{st} with respect to CO_2 loadings. The values of the b constant (Sip adsorption affinity parameter) revealed a decrease with an increase in the adsorption temperature, indicating that the AC has a

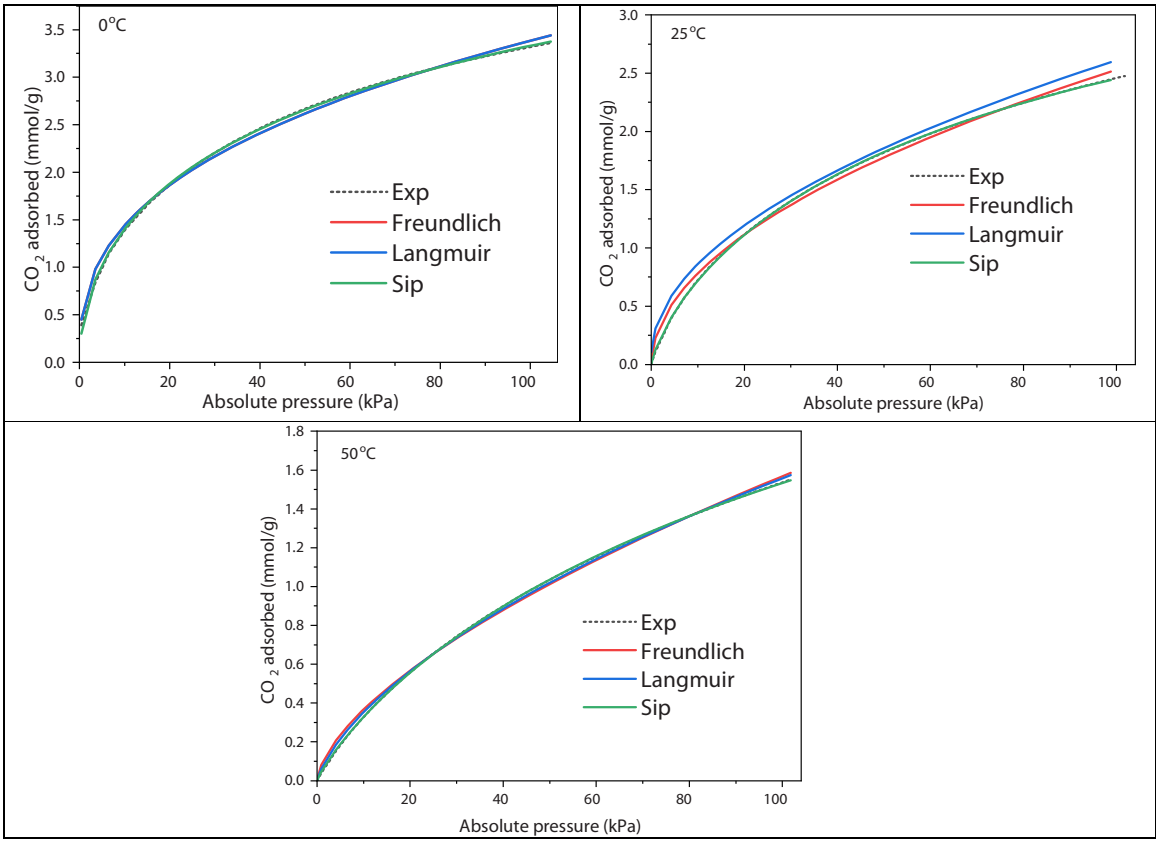

Fig. 7. CO_2 adsorption isotherms of PET-5 fitted with different adsorption models.

Table 5
Sip model fitting parameters for CO_2 adsorption isotherm at different temperatures.

Sample	Temperature (°C)	b	n	$q_{max,\ cal}/q_{max,\ expt}$ (mmol/g)	Δq (%)	R^2
PET-5	0	0.065	1.86	7.55/3.37	0.20	0.9999
	25	0.029	1.29	4.78/2.47	0.07	0.9999
	50	0.013	1.17	3.75/1.55	0.02	0.9999

b = Sips adsorption affinity constant, n = heterogeneity constant, $q_{max,\ cal}$ = from Sips model elucidated using Excel solver, $q_{max,\ expt}$ =obtained from experiment using the ASAP 2020, Δq is the residual sum of squares between the experimental uptake and that predicted by the models.

higher affinity for CO_2 at 0 °C than at 50 °C, which reveals a physisorption process and an indication of low regeneration energy. The other two models (Langmuir and Freundlich) were found to have the least goodness of fit (see Supplementary Information) when tested over the experimental values. At lower pressures of adsorption, the Sips model had previously been reported to provide the best fit for CO_2 adsorption experimental data [42,74], which agrees with the results found in this study.

4. Conclusion

MW activation time influences the yield, textural properties, and CO_2 uptake capacity of PET-derived adsorbents. A shorter MW activation time improves the yield and CO_2 uptake capacity of PET-derived adsorbents compared to a moderate or long activation time. The optimal MW activation time of 5 minutes resulted in an improved CO_2 uptake, which was found to be higher than that shown by Norit PK1–3, a commercial AC, as well as some of the published CO_2 adsorbents. Beside this, the optimal sample, PET-5, also displayed great properties as a CO_2 adsorbent, such as high thermal stability, moderate average heat of adsorption, good selectivity of CO_2 over N_2 (in a flue gas mixture of 10% CO_2/90% N_2), excellent recyclability, and cyclic stability with high regeneration efficiency (97%) over 20 repetitive adsorption-desorption cycles. This study demonstrates that promising CO_2 adsorbents with significant CO_2 uptake can be produced from a cheap, abundant, and widely accessible waste material (i.e., PET plastic), using a less concentrated KOH solution (0.72 M), a moderate activation temperature (400 °C) and a short MW activation time of 5 minutes. The short MW activation time (lower than obtained in conventional activation) and moderate activation temperature employed to produce AC in this study have outstanding transformative potential, as adsorbent materials produced from waste using this highly effective heating source (microwaves) will reduce the energy inputs on the production routes, save processing time and make AC production for CO_2 capture applications more sustainable, economically feasible and therefore more attractive.

CRediT authorship contribution statement

Claudia Fernandez Martin: Writing – review & editing, Visualization, Supervision, Resources, Project administration, Methodology, Investigation, Funding acquisition, Formal analysis, Conceptualization. **Davide Dionisi:** Writing – review & editing, Supervision, Formal analysis. **Alan J McCue:** Writing – review & editing, Visualization, Validation, Supervision, Formal analysis, Conceptualization. **Emmanuel Udo Dan:** Writing – original draft, Visualization, Validation, Methodology, Investigation, Funding acquisition, Formal analysis, Data curation.

Declaration of Competing Interest

The authors declare that they have no known competing financial interests or personal relationships that could have appeared to influence the work reported in this paper.

Data availability

No data was used for the research described in the article.

Acknowledgement

The authors would like to thank the Tertiary Education Trust Fund (TETFund), Nigeria, for funding the Doctoral programme of Emmanuel Dan at the University of Aberdeen, United Kingdom. Dr Claudia Fernández Martín acknowledges the Development Trust for the Grant 1155 awarded for the acquisition of the microwave instrument, Flex-iWave from Milestone.

Appendix A. Supporting information

Supplementary data associated with this article can be found in the online version at doi:10.1016/j.jcou.2024.102807.

References

[1] F. Nocito, A. Dibenedetto, Atmospheric CO_2 mitigation technologies: carbon capture utilization and storage, Curr. Opin. Green. Sustain Chem. vol. 21 (2020) 34–43, https://doi.org/10.1016/j.cogsc.2019.10.002.

[2] R. Hoseinzadeh Hesas, A. Arami-Niya, W.M.A. Wan Daud, J.N. Sahu, Microwave-assisted production of activated carbons from oil palm shell in the presence of CO_2 or N2 for CO_2 adsorption, J. Ind. Eng. Chem. vol. 24 (2015) 196–205, https://doi.org/10.1016/j.jiec.2014.09.029.

[3] N.M. Haimour, S. Emeish, Utilization of date stones for production of activated carbon using phosphoric acid, Waste Manag. vol. 26 (6) (2006) 651–660, https://doi.org/10.1016/j.wasman.2005.08.004.

[4] S. Deng, H. Wei, T. Chen, B. Wang, J. Huang, G. Yu, Superior CO_2 adsorption on pine nutshell-derived activated carbons and the effective micropores at different temperatures, Chem. Eng. J. vol. 253 (2014) 46–54, https://doi.org/10.1016/j.cej.2014.04.115.

[5] H.M. Coromina, D.A. Walsh, R. Mokaya, Biomass-derived activated carbon with simultaneously enhanced CO_2 uptake for both pre and post combustion capture applications, J. Mater. Chem. A Mater. vol. 4 (1) (2015) 280–289, https://doi.org/10.1039/c5ta09202g.

[6] Q. Li, S. Liu, L. Wang, F. Chen, J. Shao, X. Hu, Efficient nitrogen doped porous carbonaceous CO_2 adsorbents based on lotus leaf, J. Environ. Sci vol. 103 (2021) 268–278, https://doi.org/10.1016/j.jes.2020.11.008.

[7] J.J. Manyà, B. González, M. Azuara, G. Arner, Ultra-microporous adsorbents prepared from vine shoots-derived biochar with high CO_2 uptake and CO_2/N_2 selectivity, Chem. Eng. J. vol. 345 (January) (2018) 631–639, https://doi.org/10.1016/j.cej.2018.01.092.

[8] P.A.S. Moura, et al., Assessing the potential of nanoporous carbon adsorbents from polyethylene terephthalate (PET) to separate CO_2 from flue gas, Adsorption vol. 24 (3) (2018) 279–291, https://doi.org/10.1007/s10450-018-9943-4.

[9] A. Boonpoke, S. Chiarakorn, N. Laosiripojana, S. Towprayoon, A. Chidthaisong, "Synthesis of activated carbon and MCM-41 from bagasse and rice husk and their carbon dioxide adsorption capacity, J. Sustain. Environ. vol. 2 (October 2014) (2013) 77–81.

[10] D. Tiwari, C. Goel, H. Bhunia, P.K. Bajpai, Melamine-formaldehyde derived porous carbons for adsorption of CO_2 capture, J. Environ. Manag. vol. 197 (2017) 415–427, https://doi.org/10.1016/j.jenvman.2017.04.013.

[11] L. Rao, et al., N-doped porous carbons from low-temperature and single-step sodium amide activation of carbonized water chestnut shell with excellent CO_2 capture performance, Chem. Eng. J. vol. 359 (September 2018) (2019) 428–435, https://doi.org/10.1016/j.cej.2018.11.065.

[12] R. Bai, et al., A new nanoporous nitrogen-doped highly-efficient carbonaceous CO_2 sorbent synthesized with inexpensive urea and petroleum coke, Carbon N. Y vol. 81 (2014) 465–473, https://doi.org/10.1016/j.carbon.2014.09.079.

[13] B. Kaur, R.K. Gupta, H. Bhunia, Microporous and mesoporous materials chemically activated nanoporous carbon adsorbents from waste plastic for CO_2 capture: breakthrough adsorption study, Microporous Mesoporous Mater. vol. 282 (January) (2019) 146–158, https://doi.org/10.1016/j.micromeso.2019.03.025.

[14] J. Serafin, J. Sreńscek-Nazzal, A. Kamińska, O. Paszkiewicz, B. Michalkiewicz, Management of surgical mask waste to activated carbons for CO_2 capture, J. CO_2 Util. vol. 59 (January) (2022), https://doi.org/10.1016/j.jcou.2022.101970.

[15] Y. Ngernyen, C. Tangsathitkulchai, M. Tangsathitkulchai, Porous properties of activated carbon produced from Eucalyptus and Wattle wood by carbon dioxide activation, Korean J. Chem. Eng. vol. 23 (6) (2006) 1046–1054, https://doi.org/10.1007/s11814-006-0028-9.

[16] M.J. Kim, S.W. Choi, H. Kim, S. Mun, K.B. Lee, Simple synthesis of spent coffee ground-based microporous carbons using K_2CO_3 as an activation agent and their application to CO_2 capture, Chem. Eng. J. vol. 397 (May, p) (2020) 125404, https://doi.org/10.1016/j.cej.2020.125404.

[17] A.S. Ello, L.K.C. De Souza, A. Trokourey, M. Jaroniec, Coconut shell-based microporous carbons for CO_2 capture, Microporous Mesoporous Mater. vol. 180 (2013) 280–283, https://doi.org/10.1016/j.micromeso.2013.07.008.

[18] G. Durán-jiménez, L.A. Stevens, E.T. Kostas, V. Hernández-montoya, J.P. Robinson, E.R. Binner, Rapid, simple and sustainable synthesis of ultra-microporous carbons with high performance for CO_2 uptake, via microwave heating, Chem. Eng. J. vol. 388 (February, p) (2020) 124309, https://doi.org/10.1016/j.cej.2020.124309.

[19] H. Mao, et al., Microporous activated carbon from pinewood and wheat straw by microwave-assisted KOH treatment for the adsorption of toluene and acetone vapors, RSC Adv. (2015) 36051–36058, https://doi.org/10.1039/c5ra01320h.

[20] T. Santos, M.A. Valente, J. Monteiro, J. Sousa, L.C. Costa, Electromagnetic and thermal history during microwave heating, Appl. Therm. Eng. vol. 31 (16) (2011) 3255–3261, https://doi.org/10.1016/j.applthermaleng.2011.06.006.

[21] T.M. Alslaibi, I. Abustan, M.A. Ahmad, A.A. Foul, A review: production of activated carbon from agricultural byproducts via conventional and microwave heating, J. Chem. Technol. Biotechnol. vol. 88 (7) (2013) 1183–1190, https://doi.org/10.1002/jctb.4028.

[22] A.D. Russell, E.I. Antreou, S.S. Lam, C. Ludlow-Palafox, H.A. Chase, Microwave-assisted pyrolysis of HDPE using an activated carbon bed, RSC Adv. vol. 2 (17) (2012) 6756–6760, https://doi.org/10.1039/c2ra20859h.

[23] L. Fan, et al., Screening microwave susceptors for microwave-assisted pyrolysis of lignin: comparison of product yield and chemical profile, J. Anal. Appl. Pyrolysis vol. 142 (2019), https://doi.org/10.1016/j.jaap.2019.05.012.

[24] P. Veronesi, E. Colombini, Ö.S. Canarslan, G. Baldi, C. Leonelli, Procedure to generate a selection chart for microwave sol-gel synthesis of nanoparticles, Chem. Eng. Process. - Process. Intensif. vol. 189 (2023), https://doi.org/10.1016/j.cep.2023.109383.

[25] K.Y. Foo, B.H. Hameed, Coconut husk derived activated carbon via microwave induced activation: effects of activation agents, preparation parameters and adsorption performance, Chem. Eng. J. vol. 184 (2012) 57–65, https://doi.org/10.1016/j.cej.2011.12.084.

[26] W. Li, L. bo Zhang, J. hui Peng, N. Li, X. yun Zhu, Preparation of high surface area activated carbons from tobacco stems with K_2CO_3 activation using microwave radiation, Ind. Crops Prod. vol. 27 (3) (2008) 341–347, https://doi.org/10.1016/j.indcrop.2007.11.011.

[27] R. Hoseinzadeh Hesas, A. Arami-Niya, W.M.A. Wan Daud, J.N. Sahu, Microwave-assisted production of activated carbons from oil palm shell in the presence of CO_2 or N_2 for CO_2 adsorption, J. Ind. Eng. Chem. vol. 24 (2015) 196–205, https://doi.org/10.1016/j.jiec.2014.09.029.

[28] C. Gabriel, S. Gabriel, E.H. Grant, B.S.J. Halstead, D. Michael, P. Mingos, Dielectric parameters relevant to microwave dielectric heating, Chem. Soc. Rev. vol. 27 (3) (1998) 213–223, https://doi.org/10.1039/a827213z.

[29] S. Horikoshi, N. Serpone, 2020, , RF power semiconductor generator application in heating and energy utilization10.1007/978-981-15-3548-2.

[30] Y. Ji, T. Li, L. Zhu, X. Wang, Q. Lin, Preparation of activated carbons by microwave heating KOH activation vol. 254 (2007) 506–512, https://doi.org/10.1016/j.apsusc.2007.06.034.

[31] G. Singh, A. Maria Ruban, X. Geng, A. VinuRecognizing the potential of K-salts, apart from KOH, for generating porous carbons using chemical activation Elsevier B.V. , vol. 451 Chemical Engineering Journal2023, , 10.1016/j.cej.2022.139045.

[32] J. Bai, J. Huang, Q. Yu, M. Demir, E. Akgul, B.N. Atlay, X. Hu, L. Wang, Fabrication of coconut shell-derived porous carbons for CO_2 adsorption application, Front Chem. Sci. Eng. vol. 17 (8) (2023) 1122–1130, https://doi.org/10.1007/s11705-022-2292-6.

[33] J. Bai, J. Shao, Q. Yu, M. Demir, B.N. Atlay, T.M. Ali, Y. Jiang, L. Wang, X. Hu, Sulfur-doped porous carbon adsorbent: a promising solution for effective and selective CO_2 capture, Chem. Eng. J. vol. 479 (2024), https://doi.org/10.1016/j.cej.2023.147667.

[34] J. Bai, J. Huang, Q. Jiang, M. Demir, M. Kilic, B.N. Atlay, L. Wang, X. Hu, Synthesis and characterization of polyphenylene sulfide resin-derived S-doped porous carbons for efficient CO_2 capture, Colloids Surf. A Physicochem Eng. Asp. vol. 674 (Oct. 2023), https://doi.org/10.1016/j.colsurfa.2023.131916.

[35] J. Bai, J. Huang, Q. Jiang, M. Demir, M. Kilic, B.N. Atlay, L. Wang, X. Hu, "N-doped porous carbon derived from macadamia nutshell for CO_2 adsorption, Fuel Process. Technol. vol. 249 (2023), https://doi.org/10.1016/j.fuproc.2023.107854.

[36] E. Brunauer, S. Emmett, P.H. Teller, Adsorption of gases in multimolecular layers, J. Am. Chem. Soc. vol. 60 (1938) 309–319.

[37] K. Horvath, G. Kawazoe, Method for the calculation of effective pore size distribution in molecular sieve carbon, J. Chem. Eng. Jpn. vol. 16 (6) (1983) 470–475.

[38] S. Biti, A. Mccue, D. Dionisi, I. Graça, C.F. Martín, Sustainable microcrystalline cellulose-based activated carbons for a greener carbon capture at post-combustion conditions, Int. J. Greenh. Gas. Control vol. 125 (January) (2023), https://doi.org/10.1016/j.ijggc.2023.103876.

[39] Y. Shi, Q. Liu, and Y. He, CO 2 Capture Using Solid Sorbents. 2015. doi: 10.1007/978-1-4614-6431-0.

[40] A. Chakraborty, B.B. Saha, S. Koyama, and K.C. Ng, "On the thermodynamic modeling of the isosteric heat of adsorption and comparison with experiments," vol. 171901, 2006, doi: 10.1063/1.2360925.

[41] J.J. Carroll, Henry's law revisited, Chem. Eng. Prog. vol. 95 (1) (1999) 49–56.

[42] J. Sreńscek-Nazzal, U. Narkiewicz, A.W. Morawski, R.J. Wróbel, B. Michalkiewicz, Comparison of optimized isotherm models and error functions for carbon dioxide adsorption on activated carbon, J. Chem. Eng. Data vol. 60 (11) (2015) 3148–3158, https://doi.org/10.1021/acs.jced.5b00294.

[43] Y. Guo, C. Tan, J. Sun, W. Li, J. Zhang, C. Zhao, Porous activated carbons derived from waste sugarcane bagasse for CO_2 adsorption, Chem. Eng. J. vol. 381 (September 2019, p) (2020) 122736, https://doi.org/10.1016/j.cej.2019.122736.
[44] N. Abuelnoor, A. AlHajaj, M. Khaleel, L.F. Vega, M.R.M. Abu-Zahra, Activated carbons from biomass-based sources for CO_2 capture applications, Chemosphere vol. 282 (June, p) (2021) 131111, https://doi.org/10.1016/j.chemosphere.2021.131111.
[45] N. Álvarez-Gutiérrez, M.V. Gil, F. Rubiera, C. Pevida, Kinetics of CO_2 adsorption on cherry stone-based carbons in CO_2/CH_4 separations, Chem. Eng. J. vol. 307 (2017) 249–257, https://doi.org/10.1016/j.cej.2016.08.077.
[46] P. Ammendola, F. Raganati, R. Chirone, CO_2 adsorption on a fine activated carbon in a sound assisted fluidized bed: thermodynamics and kinetics, Chem. Eng. J. vol. 322 (2017) 302–313, https://doi.org/10.1016/j.cej.2017.04.037.
[47] G.I. Razdyakonova, O.A. Kokhanovskaya, V.A. Likholobov, Influence of environmental conditions on carbon black oxidation by reactive oxygen intermediates, Procedia Eng. vol. 113 (2015) 43–50, https://doi.org/10.1016/j.proeng.2015.07.287.
[48] S.T. Sing, K.S.W. Everett, D.H. Haul, R.A.W. Moscou, L. Pierotti, R.A. Rouquerol J, REPORTING PHYSISORPTION DATA FOR GAS/SOLID SYSTEMS with Special Reference to the Determination of Surface Area and Porosity, Pure Appl. !. Chem. vol. 57 (4) (1985) 603–619.
[49] E. Dan, A.J. McCue, D. Dionisi, C. Fernández Martín, Household mixed plastic waste derived adsorbents for CO_2 capture: a feasibility study, J. Environ. Manag. vol. 355 (Mar. 2024), https://doi.org/10.1016/j.jenvman.2024.120466.
[50] S. Biti, A. Mccue, D. Dionisi, I. Graça, C.F. Martín, Sustainable microcrystalline cellulose-based activated carbons for a greener carbon capture at post-combustion conditions, Int. J. Greenh. Gas. Control vol. 125 (March) (2023), https://doi.org/10.1016/j.ijggc.2023.103876.
[51] M. Zgrzebnicki, V. Nair, S. Mitra, R.J. Wrobel, N-doped activated carbon derived from furfuryl alcohol – development of porosity, properties, and adsorption of carbon dioxide and ethene vol. 427 (August 2021) (2022), https://doi.org/10.1016/j.cej.2021.131709.
[52] A. Czyz, R. Pietrzak, and A.W. Morawski, "MgO / CaO-Loaded Activated Carbon for Carbon Dioxide Capture: Practical Aspects of Use.," 2013.
[53] C.F. Martín, M.G. Plaza, S. García, J.J. Pis, F. Rubiera, C. Pevida, Microporous phenol-formaldehyde resin-based adsorbents for pre-combustion CO_2 capture, Fuel vol. 90 (5) (2011) 2064–2072, https://doi.org/10.1016/j.fuel.2011.01.019.
[54] J. Serafin, U. Narkiewicz, A.W. Morawski, R.J. Wróbel, B. Michalkiewicz, Highly microporous activated carbons from biomass for CO_2 capture and effective micropores at different conditions, J. CO_2 Util. vol. 18 (2017) 73–79, https://doi.org/10.1016/j.jcou.2017.01.006.
[55] Z. Yıldız, N. Kaya, Y. Topcu, H. Uzun, Pyrolysis and optimization of chicken manure wastes in fluidized bed reactor: CO_2 capture in activated bio-chars, Process Saf. Environ. Prot. vol. 130 (2019) 297–305, https://doi.org/10.1016/j.psep.2019.08.011.
[56] G.K. Parshetti, S. Chowdhury, R. Balasubramanian, Biomass derived low-cost microporous adsorbents for efficient CO_2 capture, Fuel vol. 148 (2015) 246–254, https://doi.org/10.1016/j.fuel.2015.01.032.
[57] N.M. Zawawi, F. Hamzah, M. Sarif, S.F.A. Manaf, A. Idris, Pencirian karbon teraktif menggunakan sistem pengaktifan kimia melalui ketuhar gelombang ultrasonik, Malays. J. Anal. Sci. vol. 21 (1) (2017) 159–165, https://doi.org/10.17576/mjas-2017-2101-18.
[58] S. Biti, A.J. McCue, D. Dionisi, I. Graça, C.F. Martín, Greener carbon capture using microwave heating for the development of cellulose-based adsorbents, Fuel vol. 358 (Feb. 2024), https://doi.org/10.1016/j.fuel.2023.130246.
[59] D. Tsyganov, et al., Simultaneous synthesis and nitrogen doping of free-standing graphene applying microwave plasma, Materials vol. 13 (18) (2020), https://doi.org/10.3390/MA13184213.
[60] A. Ligero, M. Calero, A. Pérez, R.R. Solís, M.J. Muñoz-Batista, M.Á. Martín-Lara, Low-cost activated carbon from the pyrolysis of post-consumer plastic waste and the application in CO_2 capture, Process Saf. Environ. Prot. vol. 173 (March) (2023) 558–566, https://doi.org/10.1016/j.psep.2023.03.041.
[61] I.P. da, P. Cansado, et al., Use of dirty plastic waste as precursors for activated carbon production—a contribution to the circular economy, Water Environ. J. vol. 36 (1) (2022) 96–104, https://doi.org/10.1111/wej.12762.
[62] S.M. Hong, S.W. Choi, S.H. Kim, K.B. Lee, Porous carbon based on polyvinylidene fluoride: Enhancement of CO_2 adsorption by physical activation, Carbon N. Y vol. 99 (2016) 354–360, https://doi.org/10.1016/j.carbon.2015.12.012.
[63] X. Yuan, S. Li, S. Jeon, S. Deng, L. Zhao, K.B. Lee, Valorization of waste polyethylene terephthalate plastic into N-doped microporous carbon for CO_2 capture through a one-pot synthesis, J. Hazard Mater. 399 (2020) 123010, https://doi.org/10.1016/j.jhazmat.2020.123010. February, p.
[64] J. Serafin, et al., Conversion of fruit waste-derived biomass to highly microporous activated carbon for enhanced CO_2 capture, Waste Manag. vol. 136 (May) (2021) 273–282, https://doi.org/10.1016/j.wasman.2021.10.025.
[65] B.C. Bai, E.A. Kim, C.W. Lee, Y.S. Lee, J.S. Im, Effects of surface chemical properties of activated carbon fibers modified by liquid oxidation for CO_2 adsorption, Appl. Surf. Sci. vol. 353 (2015) 158–164, https://doi.org/10.1016/j.apsusc.2015.06.046.
[66] J.H. Lee, H.J. Lee, J.W. Choi, Unveiling anomalous CO_2-to-N_2 selectivity of graphene oxide, Phys. Chem. Chem. Phys. vol. 19 (34) (2017) 22743–22748, https://doi.org/10.1039/c7cp04318j.
[67] M.M. Yassin, J.A. Anderson, G.A. Dimitrakis, C.F. Martín, Effects of the heating source on the regeneration performance of different adsorbents under post-combustion carbon capture cyclic operations. A comparative analysis, Sep Purif. Technol. vol. 276 (July, p) (2021) 119326, https://doi.org/10.1016/j.seppur.2021.119326.
[68] N.A. Rashidi, S. Yusup, L.H. Loong, "Kinetic studies on carbon dioxide capture using activated carbon, Chem. Eng. Trans. vol. 35 (2013) 361–366, https://doi.org/10.3303/CET1335060.
[69] N.S. Nasri, U.D. Hamza, S.N. Ismail, M.M. Ahmed, R. Mohsin, Assessment of porous carbons derived from sustainable palm solid waste for carbon dioxide capture, J. Clean. Prod. vol. 71 (2014) 148–157, https://doi.org/10.1016/j.jclepro.2013.11.053.
[70] M. Peyravi, Synthesis of nitrogen doped activated carbon/polyaniline material for CO_2 adsorption, Polym. Adv. Technol. vol. 29 (1) (2018) 319–328, https://doi.org/10.1002/pat.4117.
[71] V.C. Srivastava, M.M. Swamy, I.D. Mall, B. Prasad, I.M. Mishra, Adsorptive removal of phenol by bagasse fly ash and activated carbon: equilibrium, kinetics and thermodynamics, Colloids Surf. A Physicochem Eng. Asp. vol. 272 (1–2) (Jan. 2006) 89–104, https://doi.org/10.1016/j.colsurfa.2005.07.016.
[72] M.S.M. Zaini, M. Arshad, S.S.A. Syed-Hassan, Adsorption isotherm and kinetic study of methane on palm kernel shell-derived activated carbon, J. Bioresour. Bioprod. vol. 8 (1) (Feb. 2023) 66–77, https://doi.org/10.1016/j.jobab.2022.11.002.
[73] J. Sreńscek-Nazzal, K. Kiełbasa, Advances in modification of commercial activated carbon for enhancement of CO_2 capture, Appl. Surf. Sci. vol. 494 (July) (2019) 137–151, https://doi.org/10.1016/j.apsusc.2019.07.108.
[74] C.A. Grande, R. Blom, A. Möller, J. Möllmer, High-pressure separation of CH_4/CO_2 using activated carbon, Chem. Eng. Sci. vol. 89 (2013) 10–20, https://doi.org/10.1016/j.ces.2012.11.024.